Journal of Translational Medicine

RESEARCH

Open Access

Molecule interacting with CasL-2 enhances tumor progression and alters radiosensitivity in cervical cancer

Yun Teng[1†], Hongmei Zhao[2†], Guoqing Xue[3], Guohui Zhang[4], Yanbin Huang[1], Wei Guo[4], Kun Zou[5*] and Lijuan Zou[1*]

Abstract

Objective Cervical cancer is a common malignancy among women, and radiotherapy remains a primary treatment modality across all disease stages. However, resistance to radiotherapy frequently results in treatment failure, highlighting the need to identify novel therapeutic targets to improve clinical outcomes.

Methods The expression of molecule interacting with CasL-2 (MICAL2) was confirmed in cervical cancer tissues and cell lines through western blotting (WB) and immunohistochemistry (IHC). Siha and Hela cells were used to examine the regulatory and biological functions of MICAL2 via knockdown and overexpression experiments. Assays including MTT, colony formation, wound healing, transwell migration, and sphere formation were employed, along with WB analysis. DNA damage in irradiated cells with MICAL2 knockdown or overexpression was evaluated using the comet assay, while γ-H2AX and Rad51 protein levels were detected by WB. In vivo experiments validated the tumorigenic and radioresistance functions of MICAL2. Additionally, the relationship between MICAL2 expression and radiotherapy response was analyzed in 62 patients with cervical cancer by assessing tumor regression and MICAL2 levels six months post-treatment.

Results MICAL2 expression was significantly elevated in cervical cancer tissues and cells. Functional analyses demonstrated that MICAL2 promotes cell proliferation, migration, and invasion by activating the MAPK and PI3K/AKT pathways, as confirmed through both in vitro and in vivo experiments. Silencing MICAL2 increased DNA damage, impeded DNA repair, and enhanced radiosensitivity. Among the 62 patients with cervical cancer, elevated MICAL2 expression was associated with a lower complete response rate to radiotherapy (25.6% vs. 60.9% in those with low expression), reduced progression-free survival, and advanced cancer stage (*$p < 0.05$).

Conclusion MICAL2 plays a critical role in tumor progression and radiotherapy resistance in cervical cancer. These findings provide a foundation for developing targeted therapies to improve treatment outcomes in this population.

Keywords Cervical cancer, DNA damage, Irradiation, MICAL2, Radioresistance

†Yun Teng and Hongmei Zhao have contributed equally to this study.

*Correspondence:
Kun Zou
zoukuunk@126.com
Lijuan Zou
zoulijuanlij@163.com
Full list of author information is available at the end of the article

© The Author(s) 2025. **Open Access** This article is licensed under a Creative Commons Attribution-NonCommercial-NoDerivatives 4.0 International License, which permits any non-commercial use, sharing, distribution and reproduction in any medium or format, as long as you give appropriate credit to the original author(s) and the source, provide a link to the Creative Commons licence, and indicate if you modified the licensed material. You do not have permission under this licence to share adapted material derived from this article or parts of it. The images or other third party material in this article are included in the article's Creative Commons licence, unless indicated otherwise in a credit line to the material. If material is not included in the article's Creative Commons licence and your intended use is not permitted by statutory regulation or exceeds the permitted use, you will need to obtain permission directly from the copyright holder. To view a copy of this licence, visit http://creativecommons.org/licenses/by-nc-nd/4.0/.

Introduction

Cancer remains a significant social, public health, and economic challenge in the twenty-first century [1]. According to global statistics from 2022, approximately 20 million new cancer cases were reported, along with nearly 10 million cancer-related deaths, posing a substantial threat to human health and life expectancy [2]. Furthermore, the economic burden of cancer is considerable, with costs varying across cancer types, countries, and regions [3]. The disease also has profound familial consequences, particularly in regions such as Asia and Africa, where cancer is a leading cause of maternal orphanhood, with cervical cancer accounting for nearly half of all maternal cancers [4].

Cervical cancer is the fourth leading cause of morbidity and mortality among women globally, posing a significant public health challenge [5]. Its impact is particularly pronounced among middle-aged women in resource-limited settings [6]. The therapeutic approaches for cervical cancer include surgery, radiotherapy, chemotherapy, immunotherapy, and targeted therapy. Radiotherapy is employed across all stages of cervical cancer, with concurrent chemoradiotherapy serving as the standard treatment for locally advanced stages (IB3–IVA) [7]. Radiotherapy exerts its effects primarily by inducing DNA damage, either directly through ionizing radiation (IR) or indirectly via the generation of reactive oxygen species (ROS), ultimately leading to tumor cell death. [8]

Despite its efficacy, the variability in the phenotypic and functional characteristics of tumor-initiating cells, also known as cancer stem cells (CSCs), represents a critical barrier to treatment success. CSCs, which are known for their radioresistance, play a pivotal role in local tumor control following radiotherapy, particularly in patients with locally advanced disease [9]. Several intrinsic mechanisms contribute to this resistance, including the activation of pro-survival pathways, enhanced DNA repair capabilities, protection against oxidative stress, an unlimited capacity for self-renewal, and impaired cell cycle arrest and apoptosis. Exogenous factors, such as the hypoxic tumor microenvironment and extracellular matrix components, further support the survival of CSCs [10].

Radiotherapy resistance, particularly in patients with locally advanced cervical cancer, often results in insufficient tumor regression or short-term recurrence [11]. To address this challenge, ongoing research focuses on identifying and characterizing novel radiosensitization targets to improve the efficacy of radiotherapy for individuals diagnosed with cervical cancer.

Systemic chemotherapy remains a cornerstone in the treatment of various malignancies, including cervical cancer. It can be classified into neoadjuvant, adjuvant, and concurrent therapy, depending on its timing relative to radiotherapy. When administered concurrently with radiotherapy, systemic chemotherapy often exerts a synergistic effect [12]. However, traditional systemic chemotherapy non-selectively targets both tumor cells and normal tissue, causing substantial toxicity to rapidly dividing normal cells, such as those in the bone marrow, hair follicles, and gastrointestinal epithelium [13].

A novel approach in cancer treatment is the use of antibody–drug conjugates (ADCs), which consist of monoclonal antibodies linked to cytotoxic agents via a stable linker. These conjugates enable selective delivery of cytotoxic agents to target cells, minimizing damage to normal tissues. ADCs are currently approved by the U.S. Food and Drug Administration (FDA) for the treatment of several cancers, including breast cancer, lymphoma, multiple myeloma, gastric cancer, and ovarian cancer [14–16]. However, premature release of the cytotoxic payload into the bloodstream remains a challenge, leading to adverse effects such as hematologic toxicity, hepatotoxicity, and gastrointestinal disturbances [17]. Moreover, immune responses triggered by the monoclonal antibody component of ADCs have occasionally resulted in severe treatment-related adverse events, including fatalities [18].

To overcome these limitations, research has increasingly focused on developing safer and more efficient methods for drug delivery. Nanocarriers have emerged as a promising solution, with polymer-based nanocarriers gaining attention due to their advantageous properties, including targeted delivery, biodegradability, biocompatibility, high drug-loading capacity, and prolonged circulation time in the bloodstream [19].

The molecule interacting with CasL (MICALs) family represents an evolutionarily conserved group of proteins that regulate cytoskeletal dynamics and play essential roles in fundamental biological processes [20, 21]. Within this family, MICAL2, a multi-domain nucleoplasmic protein, facilitates F-actin depolymerization through interactions with signaling molecules such as vascular endothelial growth factor (VEGF), platelet-derived growth factor (PDGF), epidermal growth factor (EGF), fibroblast growth factor (FGF), and their respective receptors [22–25]. These interactions activate epithelial-mesenchymal transition (EMT)-related proteins via multiple pathways, thereby enhancing cancer cell metastasis [21, 26–28].

MICAL2 is overexpressed in various tumors, including gastric cancer and glioblastoma, where it contributes to tumor cell proliferation and invasion [29, 30]. Additionally, it mediates NADPH oxidation in prostate cancer and correlates with MKI67, a proliferation marker in bladder cancer, underscoring its role as a tumor promoter [21, 31, 32]. In breast cancer, elevated MICAL2 levels increase

epidermal growth factor receptor (EGFR) expression by delaying its degradation [33].

Despite these observations, the role and mechanism of MICAL2 in cervical cancer remain poorly understood and have not been fully elucidated. Preliminary evidence has identified *MICAL2* as a gene that significantly differentiates radiotherapy-resistant cervical cancer cells from normal epithelial cells. Its expression has also been validated in human tumor tissues, yet the specific mechanisms underlying its function remain unclear [34]. Consequently, this study aimed to investigate the role and mechanisms of MICAL2 in cervical cancer, with a particular focus on its impact on the radiosensitivity of the disease.

We investigated the effects of MICAL2 on cervical cancer cell proliferation and radioresistance and evaluated the relationship between MICAL2 expression levels and the clinical efficacy of radiotherapy in cervical cancer. The findings demonstrated that MICAL2 enhanced cervical cancer cell proliferation, migration, and invasion in vitro. In vivo experiments further confirmed that MICAL2 significantly increased tumor growth rate and size in cervical cancer xenograft models. Moreover, both in vitro and in vivo data indicated that MICAL2 inhibited DNA damage during radiotherapy, thereby contributing to increased radioresistance. Clinically, individuals with cervical cancer exhibiting high MICAL2 expression showed poor responses to radiotherapy. These results suggest that targeting MICAL2 may represent a promising therapeutic approach to improve radiotherapy outcomes in cervical cancer.

Materials and methods

Patients and tissue samples

This study was conducted in compliance with the Declaration of Helsinki and approved by the Ethics Committee of The Second Affiliated Hospital of Dalian Medical University (authorization code: 2023020). A total of 62 patients with International Federation of Gynecology and Obstetrics (FIGO) stage I–III cervical squamous cell carcinoma, who underwent radical pelvic radiotherapy with or without para-aortic lymph node irradiation in our department between September 2018 and September 2022, were included. All participants received standard concomitant chemoradiotherapy, and no surgical resection was performed prior to the completion of statistical analyses.

Additionally, 16 patients with cervical squamous cell carcinoma, aged 18–80 years, who underwent surgery in our hospital between 2022 and 2023 were randomly selected for inclusion. Written informed consent was obtained from all participants prior to their enrollment in the study. Tumor tissue samples, including tumor and surrounding tissues, were collected from patients who had not received anti-tumor therapy since diagnosis. All patient data were verified for accuracy.

Cell lines and culture

Human cervical cell lines Siha, HeLa, HeLa S3, C33-A, and CaSki, as well as normal cervical cells Ect1, were obtained from the American Type Culture Collection (ATCC). Cells were cultured in Dulbecco's Modified Eagle's Medium (Gibco, USA) supplemented with 10% fetal bovine serum (FBS, Gibco, USA). All cells were maintained at 37 °C in a humidified incubator with 5% CO_2.

Cellular viability assay

Cell viability was assessed using the MTT assay. Briefly, cells were seeded into a 96-well plate at a density of 2,000 cells per well. The following day, cells were transfected with various siRNAs in medium without FBS. Absorbance was measured at 490 nm using a Microplate Reader (Thermo, USA) to determine cell viability.

Western immunoblotting (WB) analysis

Proteins were extracted from cell and tissue lysates (Beyotime, Shanghai, China) and separated using 10% sodium dodecyl sulfate–polyacrylamide gel electrophoresis (SDS-PAGE). The proteins were then transferred electrophoretically to polyvinylidene fluoride (PVDF) membranes. Following transfer, the membranes were incubated with primary antibodies: MICAL2 (13965-1-AP, Proteintech, China), AKT (#4691, CST, USA), p-AKT (#13038, CST, USA), extracellular regulated protein kinases (ERK, #4695, CST, USA), p-ERK (#9154, CST, USA), P38 (#9212, CST, USA), p-P38 (#4511, CST, USA), PI3Kinase p110γ (#4249, CST, USA), p–c-Raf (#9421, CST, USA), B-cell leukemia/lymphoma 2 (Bcl-2, 12789-1-AP, Proteintech, China), BCL2-Associated X Protein (Bax, 50599-2-lg, Proteintech, China), cleaved caspase-9 (#9502, CST, USA), cleaved PARP (13371-1-AP, Proteintech, China), vimentin (#5741, CST, USA), matrix metalloproteinase 9 (MMP9, 10375-1-AP, Proteintech, China), E-cadherin (20874-1-AP, Proteintech, China), N-cadherin (22018-1-AP, Proteintech, China), Snail (#3879, CST, USA), CD44 (15675-1-AP, Proteintech, China), CD133 (184701-AP, Proteintech, China), Nanog (14295-1-AP, Proteintech, China), Ki67 (19972-1-AP, Proteintech, China), P110α (#4249P, CST, USA), γ-H2AX (#9718S, CST, USA), Rad51 (14961-1-AP, Proteintech, China), actin (20536-1-AP, Proteintech, China), and GAPDH (10494-1-AP, Proteintech, China). Protein bands were detected using enhanced chemiluminescence (ECL, Bio-Rad Laboratories, Inc., USA) based on the instructions provided by the manufacturer.

Design and transfection of siRNA

To inhibit MICAL2 expression, cells were transfected with MICAL2-specific siRNAs (SiRNA1: 5′-GCAUAG AUCUUGAGAACAUTT-3′, 5′-AUGUUCUCAAGA UCUAUGCTT-3′; SiRNA2: 5′-GCAGCGACACGU GUUACUUTT-3′, 5′-AAGUAACACGUGUCGCUG CTT-3′) or non-specific siRNA (10 μmol/L) synthesized by Suzhou GenePharma Company (China). The siRNA duplexes (2 μg) were delivered into the cells using Lipofectamine 2000 (Invitrogen, USA). Protein expression was assessed using WB, and cell viability was assessed using the MTT assay, 48 h after transfection.

Plasmid vectors and transfection

The MICAL2 plasmid was procured from OriGene (USA). Additionally, plasmids containing MICAL2 gene sequences of varying lengths were constructed in the laboratory and utilized for transfection experiments. For MICAL2 overexpression, HeLa and Siha cells were transfected with either a MICAL2-overexpressing plasmid or a LacZ control vector.

Establishment of a stable cell line

To achieve MICAL2 knockdown in HeLa and Siha cells, short hairpin RNAs (shRNAs) targeting MICAL2 were employed. Four distinct shRNA plasmids and a control plasmid containing non-targeting shRNA fused to mCherry were obtained from GeneCopoeia (Rockville, USA). Virus packaging and transfection were performed following the instructions in the Lenti-Pac™ HIV Expression Packaging Kit User Manual (GeneCopoeia). Fluorescence microscopy and WB analysis identified Sh1 (5′-GGTCAATTCATAGAAGAACTT-3′) and Sh2 (5′-GGTAAATCCCAACATGTACCA-3′) as the most effective sequences for silencing MICAL2 expression. To enhance MICAL2 expression, HeLa and Siha cells were infected with lentivirus containing the MICAL2 overexpression construct (LvOE).

Colony formation assay

Cervical cancer cells were seeded into six-well plates and transfected the following day. After 6 to 8 h of incubation in a serum-free medium, the medium was replaced with one supplemented with 10% FBS. After 48 h, cells were harvested, and 700 cells from each group were plated into separate six-well plates. The cells were cultured for 12 days, after which they were washed, fixed, and stained. Colonies containing more than 50 cells were counted under a light microscope (Olympus, Japan).

Acridine orange/ethidium bromide (AO/EB) fluorescence staining

Siha and HeLa cells were cultured on chamber slides and treated with MICAL2 siRNA. After 48 h, detached cells were collected, washed with PBS, and fixed with 95% ethanol for 15 min. Subsequently, 10 μL acridine orange/ethidium bromide (AO/EB) solution (50 μg/mL) was added to each well. Images of the cells were captured using a Leica DM 14000B microscope equipped with a digital camera. Ethidium bromide (EB) staining was used to identify damaged cell membranes, with apoptotic cells displaying increased orange-red fluorescence in their nuclei. Apoptotic cell counts were analyzed using ImageJ software.

Wound-healing and transwell migration assay

Cell migration was assessed using wound-healing and transwell assays. For the wound-healing assay, transfected cells grown in six-well plates were scratched with sterile pipette tips to create a linear gap. Images of the gaps were captured at 0, 24, 48, and 72 h post-scratch using a Leica DM 14000B microscope (Germany).

For the transwell invasion assay, transfected cells were seeded into the upper chambers of transwell inserts precoated with Matrigel (BD Biosciences, USA). Cells were incubated for 36 to 48 h, after which the invaded cells on the lower side of the membrane were fixed, stained, and observed. Cell invasion was quantified by counting the stained cells under a high-magnification light microscope.

Sphere formation

Transfected cervical cancer cells were cultured in ultralow attachment plates (Corning, USA) and suspended in serum-free DMEM/F12 supplemented with 1×B27 (Life Technologies, USA), 20 ng/mL EGF, and 10 ng/mL basic FGF (both from BD Biosciences, USA). Fresh medium was replenished three times a week. After 14 days of incubation, spheres containing more than 25 cells were counted under a light microscope.

Irradiation assay

A single dose of 4 Gy of 6 MV X-rays was delivered to cells using an X-320ix irradiator (Precision X-Ray, Inc., USA) at a dose rate of 0.40 Gy/min and a target distance of 50 cm. During radiation exposure, the cells were covered with a 1.0 cm-thick wax plate for uniform dose distribution.

For mouse irradiation, the animals were anesthetized and immobilized within a glass cage to ensure accurate targeting. Tumors were positioned at the center of the irradiation field and exposed to 6 MV X-rays (dose rate:

1.32 Gy/min, 320 keV peak, 6 mA, filtered with 2 mm Al). A dose of 2 Gy was administered daily on days 5, 7, 9, 11, 13, and 15, resulting in a total cumulative dose of 12 Gy.

Tumor cell comet assay

After transfection and X-ray irradiation, cervical cancer cells were harvested for comet assay analysis. A base layer of normal melting point agarose gel (100 μL) was applied to a microscope slide and allowed to solidify for 30 min. Subsequently, cells were suspended in low melting point agarose gel and overlaid onto the solidified base.

The slides were immersed in a chilled electrophoresis buffer (300 mM NaOH, 1 mM EDTA) and subjected to electrophoresis at 25 V for 25 min. Following electrophoresis, the slides were stained with ethidium bromide solution (20 μg/mL) and visualized using an Olympus fluorescence microscope. The percentage of DNA in the tail was calculated using the Comet Assay Software Project (CASP) according to the formula: 100 − (head fluorescent intensity / (head fluorescent intensity + tail fluorescent intensity)) × 100.

The tail length was measured as the distance between the head and the full length of the tail.

Nuclear extraction

Cells were incubated for 10 min in 250 μL of cytoplasmic lysis buffer containing 10 mM HEPES (pH 7.9), 10 mM KCl, 1.5 mM $MgCl_2 \cdot 6H_2O$, 300 mM sucrose, and 0.5% NP-40, supplemented with protease inhibitors: 10 mM NaF, 2.5 mM β-glycerophosphate, 1 mM Na_3VO_4, 0.1 mM PMSF, 1 μg/mL leupeptin, and 0.5 mM dithiothreitol. The mixture was kept on ice for 10 min, then centrifuged at 10,400 × g for 10 min at 4 °C to isolate nuclear proteins. The concentration of nuclear protein was quantified using a BCA protein assay (Beyotime, China).

Tissue microarrays

Cervical cancer tissue microarrays were obtained from Outdo Biotech, Shanghai, China. Tumor tissue specimens, encompassing both cancerous and adjacent non-cancerous tissues, were collected from patients who had not undergone any anti-tumor treatments since diagnosis. All patient information was verified for accuracy. MICAL2 protein expression levels were evaluated based on staining intensity observed in the tissue microarrays. Slides were scored according to the extent and intensity of the staining.

Immunohistochemical staining

Immunohistochemical (IHC) staining was performed using the DAB (3,3′-diaminobenzidine) Kit (Origene, China) on cervical cancer tissues, tissue microarrays, and samples from nude mice. The samples were incubated with primary antibodies at 4 °C for 12 h: MICAL2 (Abmart, 1:200), Ki67 (Proteintech, 1:50), CD133 (Proteintech, 1:50), P110α (CST, 1:150), Rad51 (Proteintech, 1:50), and γ-H2AX (CST, 1:150).

Following incubation, the slides were treated with a secondary antibody conjugated with streptavidin/peroxidase, counterstained with hematoxylin, and developed using DAB substrate. The overall expression score for each sample was calculated by multiplying the staining intensity (0 for negative staining; 1 for weak staining; 2 for moderate staining; 3 for strong staining) by the percentage of stained cells (1 for positive cells comprising ≤ 25% of the total, 2 for 26–50%, 3 for 51–75%, and 4 for > 75%). Samples with a score of 7 or higher were classified as having high expression, while those with a score below 7 were classified as having low expression.

Tumor model and tissue processing in vivo

Four-week-old female BALBc/nude mice were obtained from the Institute of Genome Engineered Animal Models for Human Disease at Dalian Medical University. All animal care and experimental procedures complied with the National Institutes of Health Guidelines for the Care and Use of Laboratory Animals and were approved by the Animal Care and Ethics Committee of Dalian Medical University (authorization code: 20233228).

Siha cells were divided into two groups (LacZ, OE), and radiotherapy-resistant Siha cells were categorized into four groups (NC, NC + IR, Sh1, and Sh1 + IR). A total of 4×10^6 cells, resuspended in cold PBS, were injected subcutaneously into the left armpit of the mice. Tumor size and body weight of nude mice were initially recorded on day 3 for the standard Siha cell group and on day 5 for the radiotherapy-resistant group. Tumor size was subsequently measured every two days using vernier calipers. The experiment was concluded on day 16 after tumor cell inoculation.

At the end of the experiment, mice were euthanized, and tumors were excised and weighed. Tumor tissues were processed as follows: a portion was quick-frozen in liquid nitrogen and stored at − 80 °C for subsequent WB analysis, while the remaining tissue was fixed in 10% formalin, embedded in paraffin, and subjected to IHC staining.

Statistical analysis

Each experiment was performed in triplicate under identical conditions. Data are expressed as mean ± standard deviation (SD), and statistical analyses were conducted using GraphPad Prism software version 5.01 (GraphPad Software, Inc., USA). Differences between test and control samples were analyzed using the Student's *t*-test,

with a p-value of less than 0.05 considered statistically significant.

Results

MICAL2 expression is elevated in cervical cancer cell lines and tumor tissues

A prior study by our group identified 59 differentially expressed genes (DEGs) between cervical cancer cells and radioresistant cervical cancer cells through RNA sequencing analysis. Among these, 42 genes were upregulated, and 17 genes were downregulated, including MICAL2 (Fig. 1A) [34]. Heat map analysis demonstrated relatively high expression levels of MICAL2 in radioresistant cervical carcinoma cell lines (Fig. 1B).

Using data from The Cancer Genome Atlas (TCGA), including cervical squamous cell carcinoma and endocervical adenocarcinoma (CESC), MICAL2 expression was further evaluated across various cancer types and adjacent normal tissues, confirming elevated expression in cervical cancer (Fig. 1C). WB analysis was performed on tumor and adjacent normal tissues from 16 patients with clinical cervical cancer. Of these samples, 10 exhibited high MICAL2 expression, while 6 showed low expression in cancer tissues (Fig. 1D). IHC staining further validated significantly elevated MICAL2 protein expression in cervical cancer tissues from 5 patient samples (Fig. 1E).

Additionally, MICAL2 expression was assessed in the normal cervical epithelial cell line Ect1 and five cervical carcinoma cell lines (Caski, C33A, HeLa, Siha, and HeLa S3). All five carcinoma cell lines displayed significantly higher MICAL2 expression compared to Ect1 (Fig. 1F).

These findings collectively demonstrate that MICAL2 is more highly expressed in cervical carcinoma tissues and cell lines than in adjacent normal tissues, suggesting its potential role in the development and progression of cervical carcinoma.

MICAL2 promotes cervical cancer cells growth and survival in vitro by inhibiting apoptosis and activating MAPK and PI3K/AKT signaling pathways

To investigate the regulatory role of MICAL2 in cervical cancer cell growth, its expression was silenced in Siha and HeLa cervical cancer cell lines, and the reduction in MICAL2 protein levels was confirmed by immunoblotting (Fig. 2A). A clonogenic assay revealed that MICAL2 knockdown significantly suppressed the clonal formation ability of Siha and HeLa cells (Fig. 2B). Similarly, the MTT assay demonstrated a significant decrease in cell viability following MICAL2 silencing in these cells (Fig. 2C).

To elucidate the molecular mechanisms underlying the role of MICAL2 in cervical cancer proliferation, its association with the PI3K/AKT and MAPK/ERK signaling pathways, which are pivotal in tumorigenesis, was evaluated. Knockdown of MICAL2 led to a marked reduction in phosphorylation levels of AKT, ERK, p38, P110r, and C-Raf (Fig. 2D), indicating that downregulation of MICAL2 inhibits proliferation by suppressing these pathways.

Apoptosis levels were further assessed using AO/EB staining, which showed an accumulation of orange-red fluorescence in the nuclei of cells with MICAL2 knockdown, indicative of increased apoptosis (Fig. 2E). Western blot analysis of apoptosis-related proteins revealed decreased Bcl-2 expression and increased levels of Bax, cleaved caspase-9 (Cl-caspase-9), and cleaved PARP (Cl-PARP) in MICAL2-silenced cells (Fig. 2F).

Conversely, overexpression of MICAL2 in Siha cells (Fig. 2G) resulted in enhanced clonogenic potential (Fig. 2H) and increased cell viability (Fig. 2I). Overexpression of MICAL2 was also associated with upregulation of phosphorylation levels for AKT, ERK, p38, P110r, and C-Raf (Fig. 2J). In line with these findings, MICAL2 overexpression reduced apoptotic cell numbers, increased Bcl-2 expression, and decreased Bax, Cl-caspase-9, and Cl-PARP levels (Fig. 2K, L).

MICAL2 enhances migration and invasion of cervical cancer cells through EMT signaling

The effect of MICAL2 on the migration and invasion capabilities of cervical cancer cells was evaluated using transwell and wound-healing assays in HeLa and Siha cells. In the transwell assay, the number of invading and migrating cells was significantly reduced in the MICAL2

(See figure on next page.)

Fig. 1 MICAL2 exhibits high expression levels in cervical cancer cell lines and tumor tissues. **A** RNA sequencing analysis demonstrates MICAL2 as one of the 59 differential genes between cervical cancer cells and radioresistant cervical cancer cells. **B** Heatmap reveals that RRSiHa and RRHeLa share 42 significantly upregulated genes, including MICAL2, when compared to their parental Siha and Hela cell lines ($n = 3$). **C** Analysis of TCGA pan-cancer data demonstrates MICAL2 expression across various cancer types, with CESC highlighted in red. **D** WB analysis confirms elevated MICAL2 expression in tumor tissues (T) compared to normal tissues (N) from 16 patients with cervical cancer. **E** Immunohistochemical (IHC) analysis further demonstrates MICAL2 expression in cancerous and adjacent tissues from 16 patients with cervical cancer, with representative morphograms presented for three cases and quantitative analysis provided for all 16 cases in a histogram. **F** WB analysis reveals MICAL2 protein expression in one normal cervical cell line and five cervical cancer cell lines ($n = 3$). Data are presented as mean ± standard deviation, with statistical significance indicated as $^{*}p < 0.05$, $^{**}p < 0.01$, and $^{***}p < 0.001$ compared to the control group

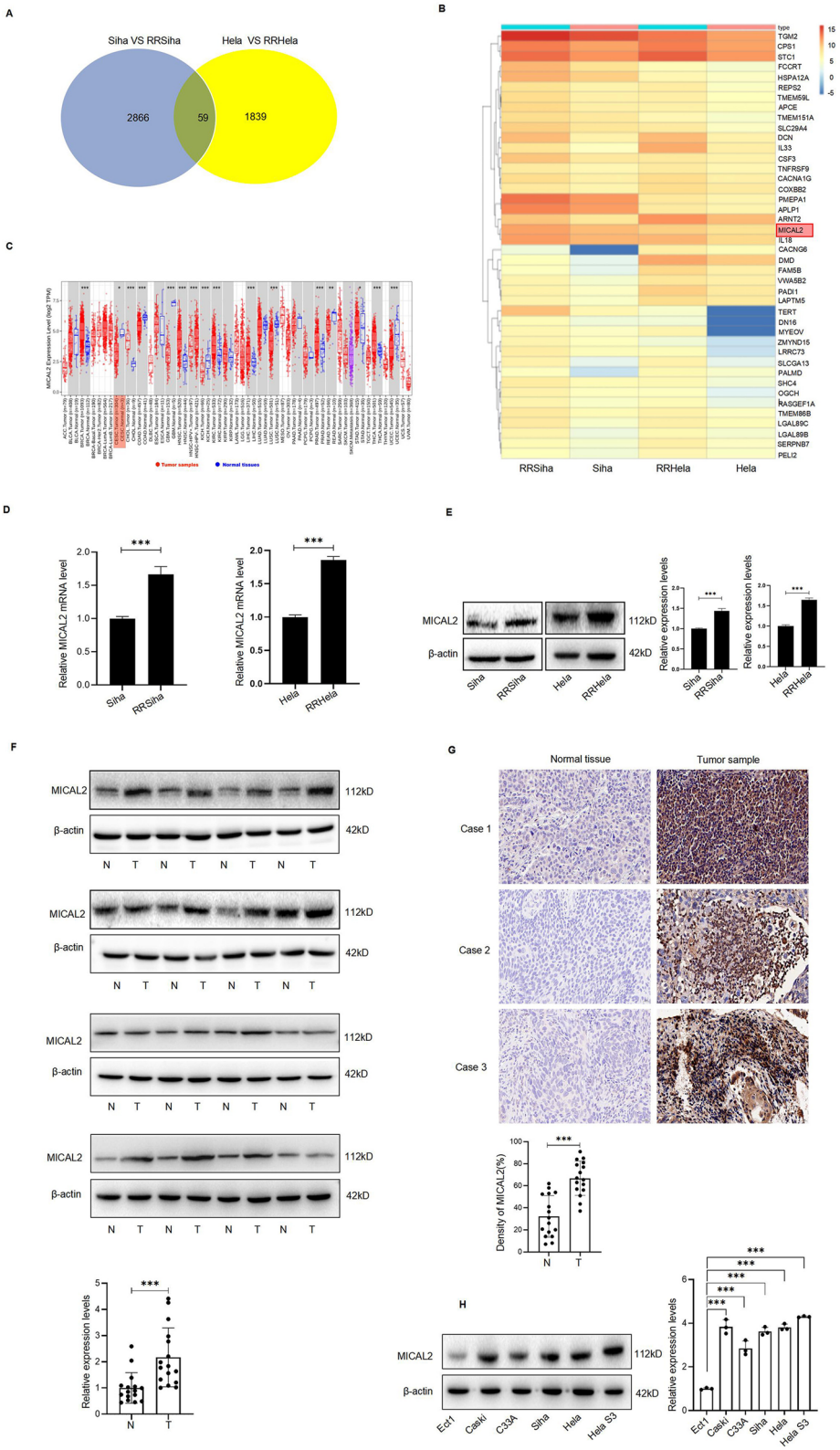

Fig. 1 (See legend on previous page.)

knockdown group compared to the siRNA control group (Fig. 3A). Similarly, in the wound-healing assay, cells with MICAL2 knockdown exhibited slower migration and a markedly lower wound closure rate at 48 h compared to the control group (Fig. 3B). These findings demonstrate that MICAL2 knockdown significantly impairs the migration and invasion abilities of cervical cancer cells.

This observation was further supported by WB analysis, which revealed changes in the expression of proteins related to the EMT pathway. Specifically, knockdown of MICAL2 resulted in reduced expression of vimentin, MMP-9, N-cadherin, and Snail, while E-cadherin expression was upregulated (Fig. 3C). Conversely, overexpression of MICAL2 in Siha cells led to enhanced invasiveness and migratory capacity (Fig. 3D–F). These results indicate that MICAL2 promotes the migration and invasion of cervical cancer cells, potentially through the activation of EMT signaling pathways.

MICAL2 promotes stem cell-like traits and tumor formation in cervical cancer cells

CSCs contribute to the progression of malignancies due to their distinctive capabilities [35]. To evaluate the involvement of MICAL2 in CSC-related traits, a sphere formation assay was performed. MICAL2 knockdown significantly reduced the sphere diameter in both SiHa and HeLa cells (Fig. 4A). Furthermore, the expression of key CSC markers, including CD133, CD44, and Nanog, was markedly downregulated in the MICAL2 knockdown group (Fig. 4B). To further explore the functional role of MICAL2, a MICAL2 overexpression plasmid was constructed and transfected into SiHa cells using a lentivirus packaging system, with the parental cell line serving as a control. WB analysis confirmed successful overexpression of MICAL2 (Fig. 4C). Compared to the knockdown results, overexpression of MICAL2 in SiHa cells led to enhanced sphere formation and increased expression of CSC markers (Fig. 4D and E). These findings collectively indicate that MICAL2 promotes stem-like characteristics in cervical cancer cells.

The regulatory role of MICAL2 in tumor growth was further investigated using a cervical carcinoma xenograft model. SiHa cells with stable MICAL2 overexpression and control cells were subcutaneously injected into the right axillary region of nude mice. The animals were divided into two groups: the MICAL2 overexpression (OE) group and the control (LacZ) group. Tumor weight and volume were measured on days 3, 5, 7, 9, 11, 13, and 15 post-inoculation. The OE group exhibited a significant increase in tumor size and weight compared to the control group (Fig. 4F and G), suggesting that MICAL2 overexpression significantly enhances tumor growth. WB and IHC analyses demonstrated that MICAL2 overexpression substantially elevated the expression of Ki67, CD133, and P110α in the cervical cancer xenografts (Fig. 4H and I). These in vivo findings align with the in vitro results, further confirming that MICAL2 overexpression promotes cervical cancer cell proliferation and tumor formation. Collectively, these results underscore the critical role of MICAL2 in fostering tumor development in cervical carcinoma.

MICAL2 reduces DNA damage and radiosensitivity of cervical cancer cells under irradiation

MICAL2 was identified as one of the 59 differentially expressed genes between cervical carcinoma cells and their radioresistant counterparts through RNA sequencing analysis [19]. However, the specific role of MICAL2 in modulating radiosensitivity in cervical carcinoma requires further investigation. Stable MICAL2 knockdown in SiHa and HeLa cells (Fig. 5A) was achieved, followed by exposure to 4 Gy irradiation. Colony formation assays demonstrated that MICAL2 knockdown inhibited the proliferation of cervical carcinoma cells and increased their radiosensitivity (Fig. 5B). In the comet assay, a significant elongation of

(See figure on next page.)

Fig. 2 MICAL2 promotes the growth and survival of cervical cancer cells in vitro, associated with apoptosis inhibition and activation of the MAPK and PI3K/AKT signaling pathways. **A** WB analysis was used to assess MICAL2 expression in Siha and Hela cells transfected with MICAL2-specific siRNAs (si-MICAL2-1 and si-MICAL2-2). **B** Colony formation assays were performed on Hela and Siha cells transfected with MICAL2 siRNA or non-specific control siRNA, with colonies greater than 50 μm counted after 14 days. **C** Cell viability of Hela and Siha cells was measured using the MTT assay following MICAL2 knockout. **D** WB analysis of proteins involved in the MAPK and PI3K/AKT pathways was conducted 48 h after transfection with MICAL2 siRNA or control siRNA. **E** AO/EB fluorescence staining was used to detect apoptotic cells in Siha and Hela cells transfected with MICAL2-specific siRNAs. **F** WB analysis assessed the effects of MICAL2 siRNA (siRNA1, siRNA2) on apoptosis-related proteins Bcl-2, Bax, cleaved caspase-9 (Cl-casp-9), and cleaved PARP (Cl-PARP) in Siha and Hela cell lines. **G**–**I** Following transfection with a MICAL2 overexpression plasmid, WB, colony formation assays, and MTT assays were conducted to confirm MICAL2 protein overexpression in Siha cells and assess the number of cell colonies and cell viability. **J** WB analysis was used to verify the effects of MICAL2 overexpression on MAPK and PI3K/AKT pathway proteins in Siha cells. **K**–**L** AO/EB staining and WB analysis was performed to detect apoptotic cells and apoptosis-related proteins (Bcl-2, Bax, Cl-casp-9, Cl-PARP) in MICAL2-overexpressing Siha cells, respectively. Data are presented as the mean ± standard deviation from three independent experiments, with statistical significance indicated as $*p < 0.05$, $**p < 0.01$, and $***p < 0.001$ compared to the control group

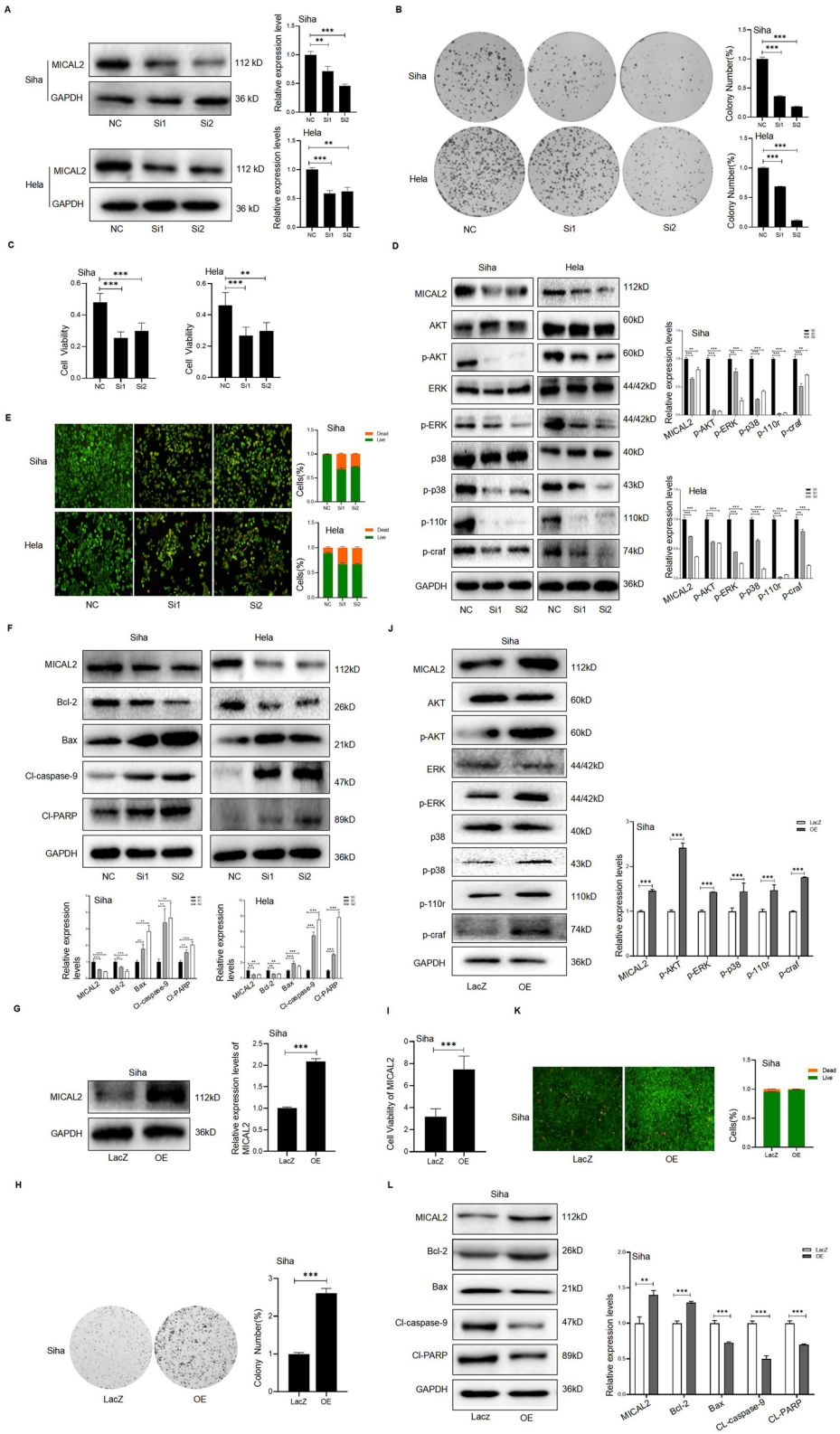

Fig. 2 (See legend on previous page.)

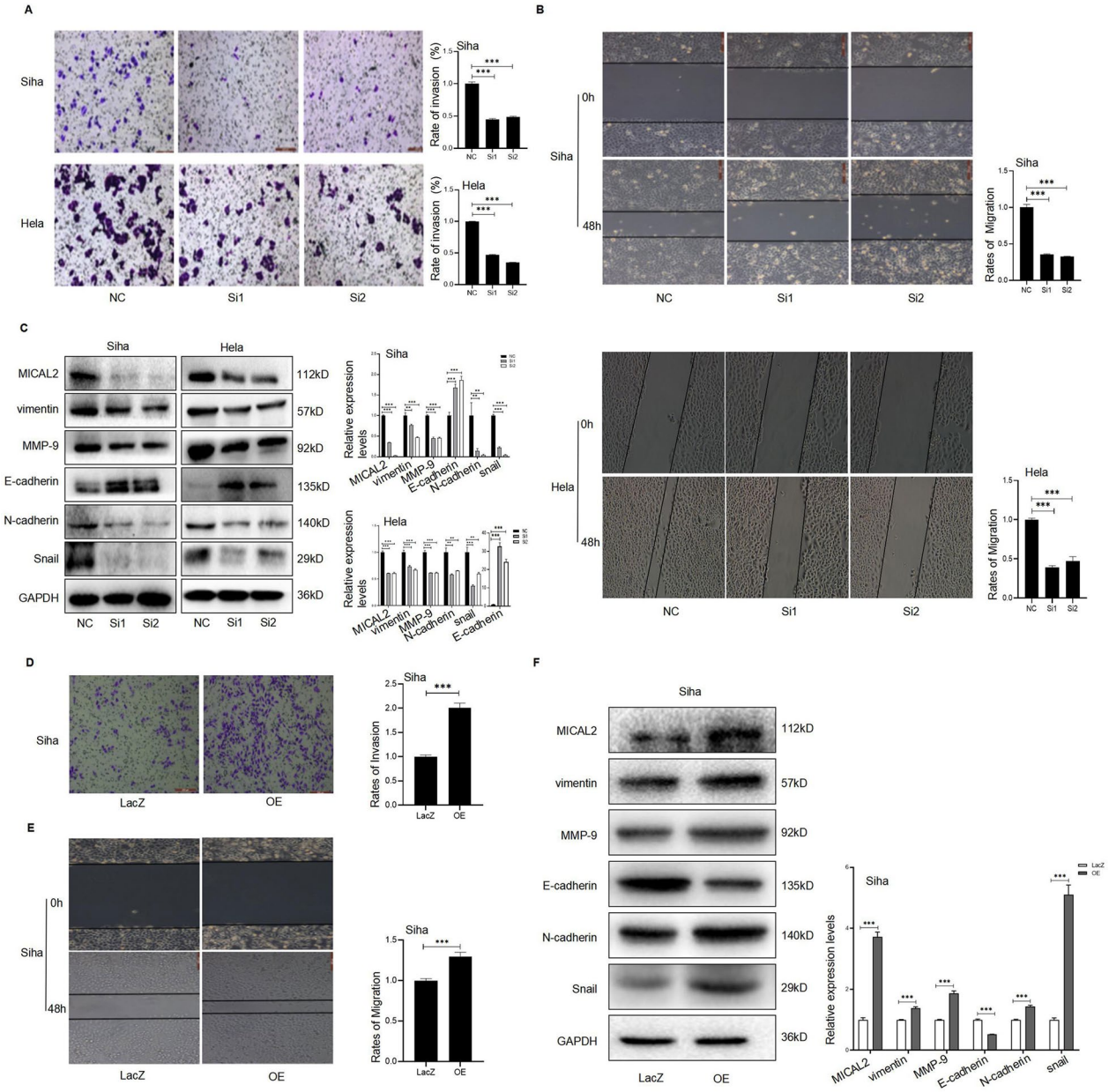

Fig. 3 MICAL2 enhances the migration and invasion of cervical cancer cells, with involvement of EMT signaling. **A** Hela and Siha cells transfected with MICAL2 siRNA1 or siRNA2 seeded in chambers coated with a diluted Matrigel matrix. The invasive cells were stained and imaged at 40 × magnification, with quantitative analysis of the invading cells presented in the histogram. **B** Cell migration assessed using a wound-healing assay. Hela and Siha cells were plated in 6-well plates, scratched with a 100 µL pipette tip, and cultured for 48 h before photographic recording. The histogram reveals the calculated cell mobility. **C** WB analysis used to measure the expression levels of vimentin, MMP-9, E-cadherin, N-cadherin, and Snail in Hela and Siha cells. **D**, **E** The invasion and migration abilities of Siha cells transfected with a MICAL2 overexpression plasmid assessed by transwell assay and wound-healing assay (×40). **F** The impact of MICAL2 overexpression on the protein levels of vimentin, MMP-9, E-cadherin, N-cadherin, and Snail in the Siha cervical cancer cell line assessed by WB. Data are presented as the mean ± standard deviation. Statistical significance is indicated as $*p < 0.05$, $**p < 0.01$, and $***p < 0.001$ compared to the control group

comet tails was observed in the MICAL2 knockdown cells (Fig. 5C), indicating greater double-stranded DNA damage and reduced DNA repair capacity following irradiation (Fig. 5D). These results were corroborated by increased activation of the DNA damage marker γ-H2AX and reduced expression of the DNA repair protein Rad51 in the MICAL2 knockdown group (Fig. 5D).

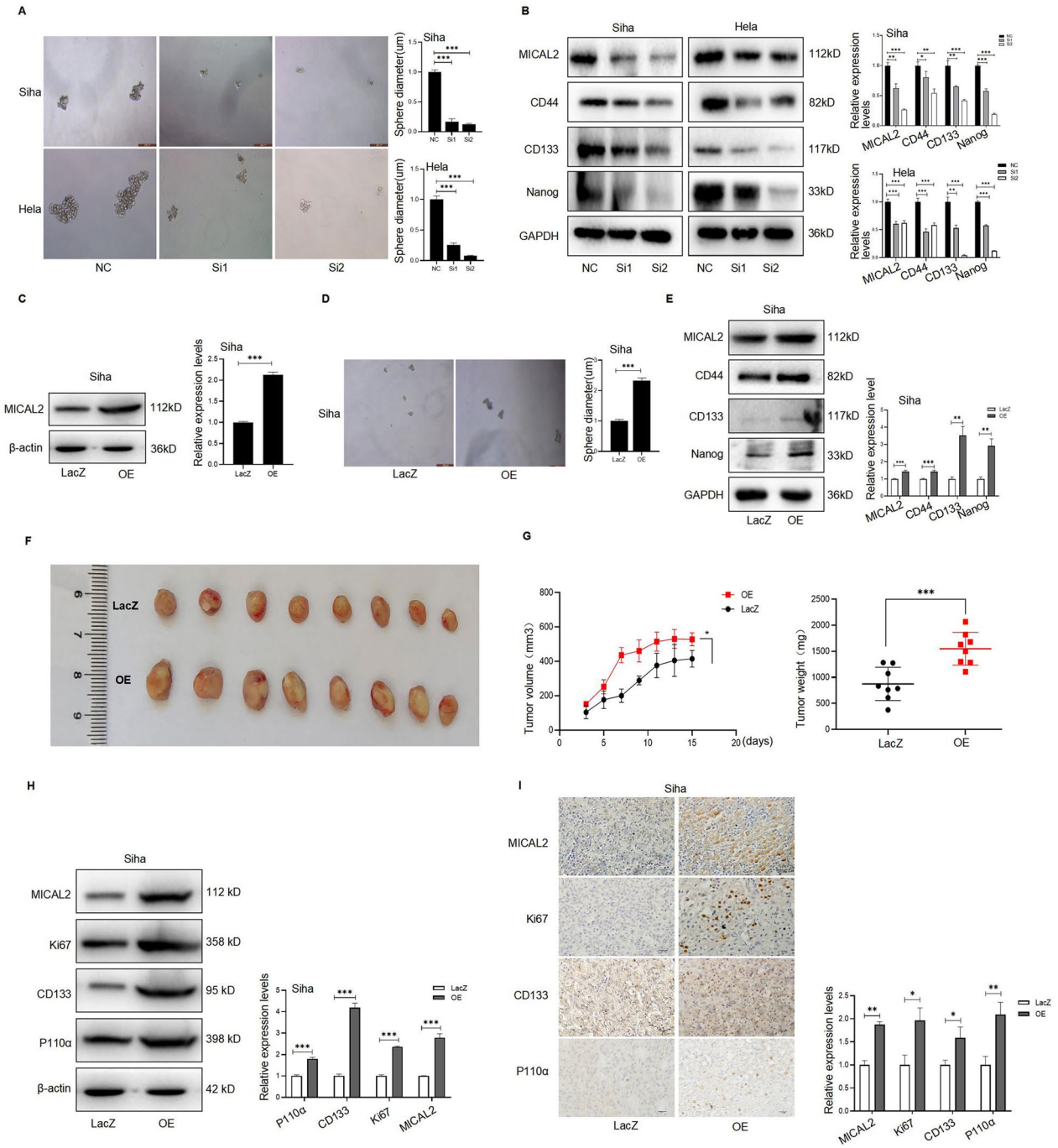

Fig. 4 MICAL2 enhances stem cell-like properties and tumor formation in cervical cancer cells. **A** The impact of MICAL2 knockdown on stemness assessed using a spheroid formation assay. Cells with MICAL2 knockdown produced significantly smaller spheroids compared to controls, indicating a reduced spheroidization capability. **B** WB analysis employed to assess the expression levels of stemness-related proteins CD44, CD133, and Nanog in Hela and Siha cells following MICAL2 knockdown. **C** Stable overexpression of MICAL2 in Siha cells verified by WB after transfection with either a non-specific control LacZ plasmid or a MICAL2 overexpressing plasmid (OE). **D**, **E** The stemness of Siha cells transfected with the MICAL2 overexpressing plasmid assessed by spheroid formation assay and WB analysis of stemness-related proteins (CD44, CD133, and Nanog). **F** Tumor cells from the LacZ control group and the MICAL2 overexpression group implanted into the right axilla of female nude mice. Xenografts were collected 15 days post-implantation, and images of the tumor tissues from both groups were captured. **G** Volume and weight of xenografts in nude mice ($n=8$) measured and compared. **H**, **I** WB and immunohistochemical analysis performed to detect the expression of key proteins Ki67, CD133, and P110α in the xenografts. Data are presented as the mean ± standard deviation. Statistical significance is indicated as $^{*}p<0.05$, $^{**}p<0.01$, and $^{***}p<0.001$ compared to the control group

Subsequently, Siha and Hela cells with stable MICAL2 knockdown were placed in 6 cm Petri dishes and subjected to varying doses of X-ray irradiation (0 Gy, 2 Gy, 4 Gy, 6 Gy, 8 Gy) to assess their potential to form clones. A survival curve was plotted based on colony counts (Fig. 5E), revealing a dose-dependent decrease in cell survival in the MICAL2 knockdown group. Conversely, when MICAL2 was overexpressed (Fig. 5F), the opposite effect was observed in the colony formation assay (Fig. 5G), comet assay (Fig. 5H), and in the protein expression levels of γ-H2AX and Rad51 (Fig. 5I). These findings indicate that MICAL2 enhances radiosensitivity in cervical cancer cells by interfering with DNA damage and repair mechanisms.

To further validate the role of MICAL2 in radioresistant cervical cancer, radiotherapy-resistant SiHa and HeLa cell lines (RRSiHa and RRHeLa) were established. Parental cells were subjected to daily X-ray irradiation at 2 Gy per session for 15 consecutive days, totaling 30 Gy. Surviving cells were collected and confirmed to exhibit radiotherapy resistance. RNA sequencing and immunoblot analyses showed significantly elevated MICAL2 expression in RRSiHa and RRHeLa cells compared to their non-resistant counterparts (Fig. 5J). Stable knockdown of MICAL2 was subsequently performed in these radiotherapy-resistant cells using lentiviral shRNA (Fig. 5K). Following 4 Gy X-ray irradiation, MICAL2 knockdown in RRSiHa and RRHeLa cells resulted in a marked reduction in proliferation (Fig. 5L), elongated comet tails (Fig. 5M), increased γ-H2AX expression, and decreased Rad51 expression (Fig. 5N).

Collectively, these findings indicate that MICAL2 modulates DNA damage and repair mechanisms, thereby reducing radiosensitivity in cervical cancer cells, including those with acquired resistance to radiotherapy.

MICAL2 knockdown inhibits cervical cancer progression in a mouse model

An in vivo xenograft experiment was conducted to investigate the role of MICAL2 in modulating radiosensitivity in cervical cancer. RRSiHa cells with stable MICAL2 knockdown and control cells were subcutaneously implanted into the axillary region of nude mice. The mice were assigned to four groups: the radiotherapy-resistant cervical cancer RRSiHa control group (RR + NC), the RRSiHa group with stable MICAL2 knockdown (RR + Sh1), the RRSiHa control group subjected to ionizing radiation (RR + NC + IR), and the RRSiHa group with stable MICAL2 knockdown subjected to radiotherapy (RR + Sh1 + IR). Mice in the radiotherapy groups received ionizing radiation at a dose of 2 Gy on days 5, 7, 9, 11, 13, and 15 after tumor implantation. Tumor size was monitored throughout the experiment (Fig. 6A).

On day 17, the mice were euthanized, and the xenograft tumors were excised for measurements of tumor size and weight (Fig. 6B and C). Consistent with in vitro findings, WB and IHC analyses revealed that MICAL2 knockdown increased the expression of the DNA damage marker γ-H_2AX and reduced the expression of Rad51 in xenograft tumors (Fig. 6D and E). These results further highlight the critical role of MICAL2 in cervical cancer progression. By increasing susceptibility to DNA damage and enhancing radiosensitivity, MICAL2 knockdown demonstrates a potential therapeutic strategy for improving the efficacy of radiotherapy in cervical cancer.

High MICAL2 expression correlates with poor clinical response to radiotherapy in patients with cervical cancer

This study examined the relationship between MICAL2 expression and radiosensitivity in cervical cancer by recruiting 62 patients diagnosed with the disease. All participants received standard concurrent chemoradiotherapy, and treatment efficacy was evaluated by at least two attending physicians using established criteria for the

(See figure on next page.)

Fig. 5 MICAL2 reduces both the DNA damage and the radiosensitivity of cervical cancer cells exposed to irradiation. **A** Cervical cancer Siha and Hela cell lines with stable MICAL2 knockdown established using MICAL2 lentiviral particles shRNA1 and shRNA2, with successful knockdown confirmed using WB analysis. **B** A colony formation assay conducted to assess the proliferation ability of Siha and Hela cells in both control and MICAL2 knockdown groups following 4 Gy X-ray irradiation. **C**, **D** Following MICAL2 shRNA transfection and 4 Gy X-ray exposure, cells were collected 6 h post-irradiation. DNA damage assessed using the comet assay, and expression levels of DNA damage marker (γ-H2AX) and repair protein (Rad51) analyzed using WB. **E** MICAL2 shRNA-treated Hela and Siha cells exposed to varying doses of X-rays (0, 2, 4, 6, and 8 Gy) for 48 h, and clonogenic survival curves generated. **F** MICAL2 overexpression in cervical cancer Siha cells achieved through MICAL2 plasmid transfection and confirmed using WB. **G**–**I** The effects of MICAL2 overexpression on cell proliferation, DNA damage, γ-H2AX, and Rad51 expression in Siha cells exposed to 4 Gy X-ray irradiation assessed using colony formation assays, comet assays, and WB. **J** Siha and Hela cells subjected to continuous low-dose X-ray irradiation (2 Gy/day for 15 days, totaling 30 Gy) to generate radioresistant cell lines (RRSiha and RRHeLa). MICAL2 expression assessed in both parental and radioresistant cells using WB. **K** Stable MICAL2 knockdown in RRSiha and RRHeLa cells was confirmed using WB. **L**–**N** The proliferation, DNA damage, and expression levels of γ-H2AX and Rad51 in RRSiha and RRHeLa cells with and without MICAL2 knockdown, following 4 Gy X-ray irradiation for 12 h, assessed using colony formation assays, comet assays, and WB. Data are presented as the mean ± standard deviation. Statistical significance is indicated as $*p < 0.05$, $**p < 0.01$, and $***p < 0.001$ compared to the control group

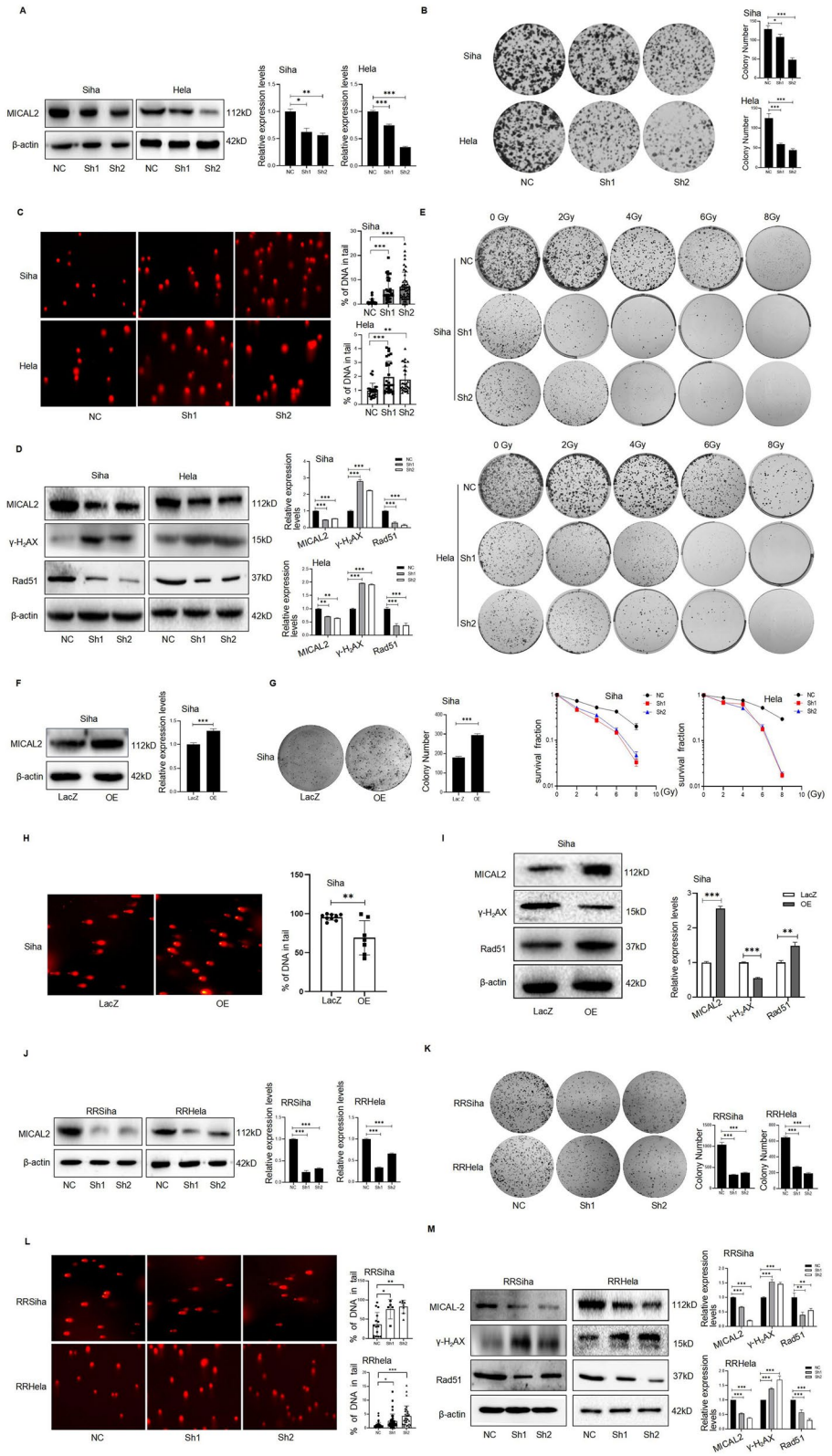

Fig. 5 (See legend on previous page.)

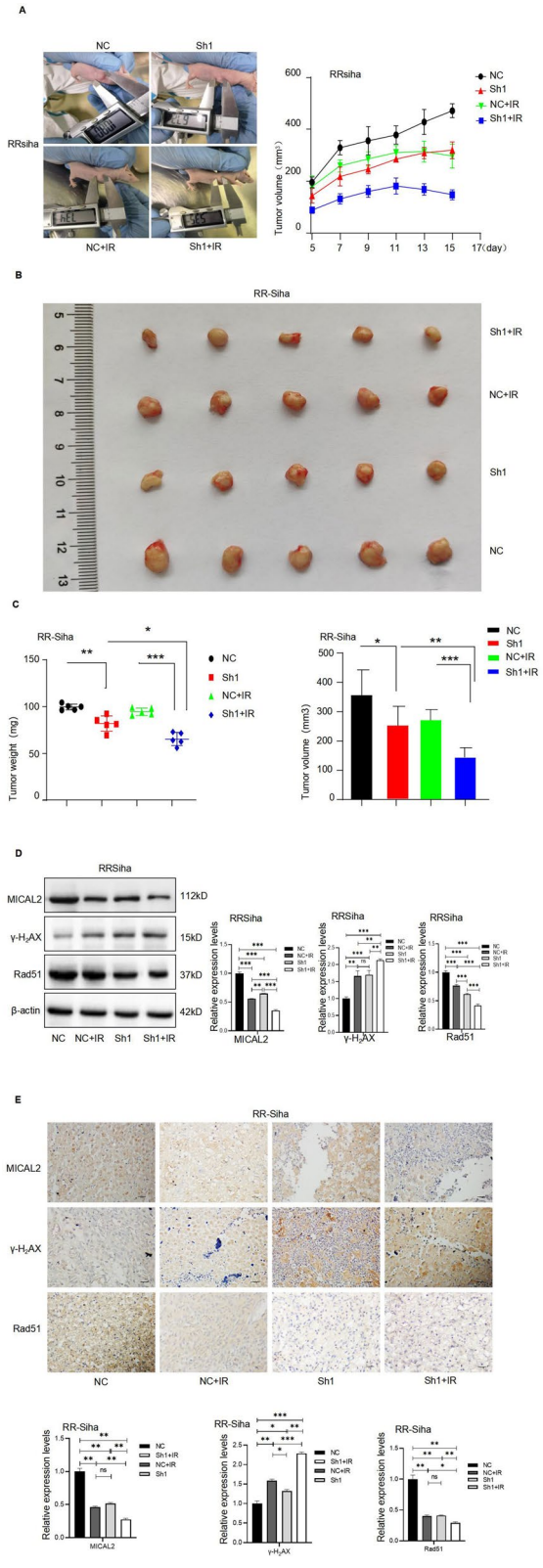

◀ **Fig. 6** MICAL2 knockdown impedes cervical cancer progression in a mouse model. Four types of cells used for subcutaneous implantation into nude mice: radiotherapy-resistant cervical cancer RRSiha cells (RR + NC), RRSiha cells with stable MICAL2 knockdown (RR + Sh1), RRSiha cells subjected to ionizing radiation (RR + NC + IR), and RRSiha cells with stable MICAL2 knockdown receiving radiotherapy (RR + Sh1 + IR). Xenograft tumors harvested 15 days post-treatment. **A**, **B** Tumor size measurements and images of xenografts are provided for each group ($n = 5$). **C** Tumor weight and volume comparisons across the different treatment groups. **D**, **E** WB and immunohistochemical analyses performed to assess the expression of γ-H2AX and Rad51 in xenograft tissues ($n = 3$). Data are expressed as the mean ± standard deviation. Statistical significance is indicated as $^{*}p < 0.05$, $^{**}p < 0.01$, and $^{***}p < 0.001$ compared to the control group

assessment of solid tumors. Six months post-radiotherapy, treatment responses were categorized as follows: 38 patients achieved a complete response (CR), 17 exhibited a partial response (PR), and 7 experienced stable disease (SD) or progressive disease (PD) (Fig. 7A).

IHC was employed to measure MICAL2 expression levels in tumor tissues. Analysis of clinical data, imaging, and IHC results (Fig. 7B) revealed that patients with high MICAL2 expression displayed limited tumor volume reduction, whereas those with low MICAL2 expression demonstrated significant tumor shrinkage or complete remission. These findings suggest that elevated MICAL2 expression is associated with poorer clinical responses to radiation therapy, and this association was positively correlated with the FIGO stage (Table 1).

Progression-free survival (PFS) and overall survival (OS) were also analyzed. Patients with low MICAL2 expression exhibited significantly longer PFS and improved tumor control. However, differences in OS between the groups did not reach statistical significance, potentially due to the small cohort size and limited duration of follow-up (Fig. 7C).

These results indicate that MICAL2 expression serves as a predictive biomarker for radiosensitivity in cervical cancer.

Discussion

This study identifies several critical findings regarding the role of MICAL2 in cervical cancer: (1) MICAL2 is a promising therapeutic target, with its high expression correlating with tumor progression and resistance to radiotherapy. (2) MICAL2 influences tumor biological behavior through the activation of the MAPK and PI3K/AKT signaling pathways, facilitating the proliferation, migration, and invasion of cervical cancer cells. (3) High MICAL2 expression is associated with inferior responses to radiotherapy in patients with cervical cancer,

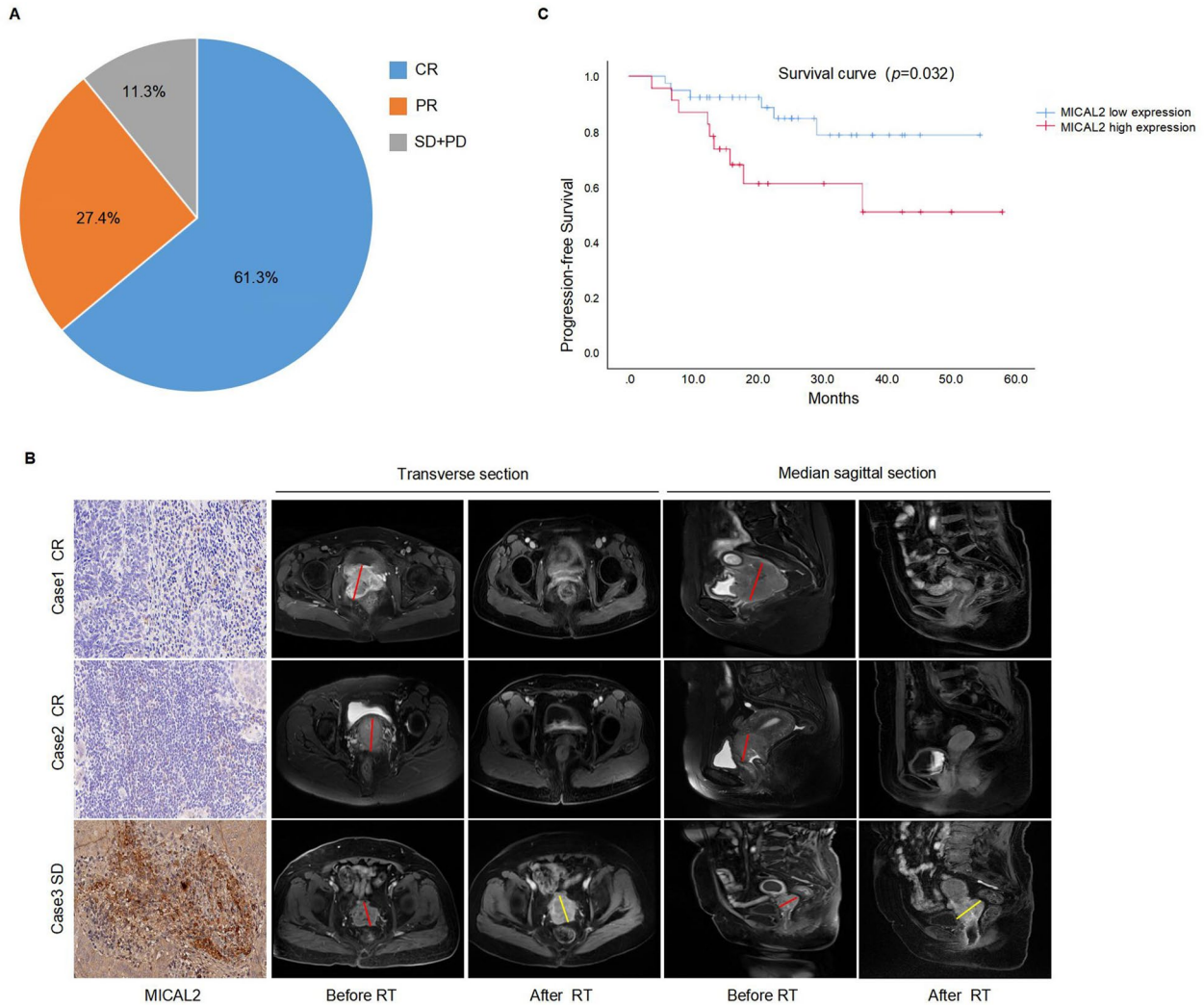

Fig. 7 Patients with cervical cancer having high MICAL2 expression exhibited poor clinical response to radiotherapy. **A** Among the 62 patients with cervical cancer who underwent radiotherapy, 38 patients achieved a complete response (CR), 17 patients had a partial response (PR), and 7 patients either had stable disease (SD) or experienced disease progression (PD) six months post-radiotherapy. **B** MICAL2 expression levels in cervical cancer tissues from 2 cases with CR and 1 case with SD, along with their corresponding MRI images (transverse and median sagittal sections) taken before and after radiotherapy. **C** Kaplan–Meier survival analysis with log-rank test used to assess disease-free progression (DFS) in patients with cervical cancer based on different MICAL2 expression levels ($n = 62$)

highlighting its potential utility as a predictive biomarker for treatment outcomes.

Concurrent chemoradiotherapy is currently the standard treatment for locally advanced cervical cancer. However, radiation resistance remains a significant factor in tumor recurrence, with OS rates ranging from 60 to 65% for stage IIB to 25 to 50% for stages III–IV cervical cancer [36, 37]. As such, elucidating the mechanisms of radiation resistance and identifying potential therapeutic targets is of critical importance.

This study demonstrates that MICAL2 contributes to cervical cancer progression and reduces radiosensitivity in cancer cells. Additionally, MICAL2 expression was found to be positively correlated with the FIGO stage of cervical cancer and inversely associated with both local tumor control and PFS. These findings suggest that targeting MICAL2 could be a promising strategy for developing novel therapeutic interventions to enhance treatment efficacy and overcome radiation resistance in cervical cancer.

The MICAL family consists of proteins characterized by several conserved domains: an N-terminal flavin monooxygenase (MO) domain, Lin11, Isl-1, and Mec-3 (LIM) domains, a calmodulin homologous (CH)

Table 1 Correlation analysis of MICAL2 protein expression with clinicopathological variables was conducted in a group of 62 patients with cervical cancer

Character	MICAL2		P value
	High (%)	Low (%)	
Age			
≤ 60	13 (56.5)	22 (56.4)	0.993
> 60	10 (43.5)	17 (43.6)	
Local control			
CR	9 (39.1)	29 (74.4)	0.006*
NCR	14 (60.9)	10 (25.6)	
FIGO stage			
I	1 (4.3)	12 (30.8)	
II	6 (26.1)	6 (15.4)	0.039*
III	16 (69.6)	21 (53.8)	
N stage			
N0	13 (56.5)	25 (64.1)	0.554
N +	10 (43.5)	14 (35.9)	
Differentiation			
Middle	5 (21.7)	8 (20.5)	
Low	8 (34.8)	15 (38.5)	1.000
Unknown	10 (43.5)	16 (41.0)	

* $P < 0.05$

The results indicate that MICAL2 expression is significantly associated with clinical pathology (*$P < 0.05$). Specifically, high MICAL2 expression was observed in 23 cases, representing 37.1% of the total sample. Pearson's chi-square test revealed a significant correlation between elevated MICAL2 expression and both the local control rate and FIGO staging ($P < 0.05$), indicating that MICAL2 may play a key role in disease progression and treatment outcomes in cervical cancer

domain, and a C-terminal coil (CC) domain. Together, these domains contribute to an auto-inhibitory mechanism that limits the production of reactive oxygen species (ROS) [38]. The family includes Drosophila Mical and three vertebrate members: MICAL-1, MICAL-2, and MICAL-3 [39]. Among these, MICAL2 is unique due to its lack of a CC domain, enabling ROS production via its MO domain without autoinhibitory regulation. This property allows MICAL2 to regulate cytoskeletal dynamics and ROS generation [38, 40].

MICAL2 has been identified as a tumor promoter in various cancers, including prostate [31], breast [33], stomach [41], and colon cancer [42]. It is frequently overexpressed in aggressive, poorly differentiated epithelial carcinomas and in cancer-associated neoangiogenic endothelial cells, underscoring its role in tumor progression [43]. Recent studies have shown that MICAL2 enhances the proliferation, migration, invasion, and EMT of lung adenocarcinoma cells via the AKT and myosin-9 pathways [28] Furthermore, it has been associated with increased chemoresistance and higher mortality in patients with endometrial cancer [44]. Although the precise mechanisms through which MICAL2 promotes cancer cell invasion and proliferation remain incompletely understood, it has been shown to activate ERK1/2 signaling to facilitate vascular smooth muscle cell growth [45]. In breast cancer, MICAL2 stabilizes EGFR and activates EGFR/P38 signaling, enhancing cell migration [33, 46].

MICAL2 also utilizes NADPH to generate ROS through its MO domain, activating pathways such as Wnt/β-catenin and Sema/Plexin, which further drive EMT in tumor cells [24]. This study confirms that MICAL2 is significantly expressed in cervical cancer cell lines and tissues. Both in vitro and in vivo experiments demonstrate that MICAL2 promotes cervical cancer cell proliferation through the MAPK and PI3K/AKT signaling pathways. These findings position MICAL2 as a potential therapeutic target in the development and progression of cervical cancer.

Irradiation resistance in tumor cells emerges from a combination of selective cell death and mutational events induced by radiotherapy. Differences in the intracellular environments of distinct cell subsets, or even within the same subpopulation, contribute to the persistence and proliferation of irradiation-tolerant cells following the elimination of radiosensitive cells. Additionally, irradiation can induce mutations in tumor cells, leading to the development of a radioresistant phenotype that can be inherited by subsequent generations [47]. Several factors influence radiotherapy sensitivity, including tumor heterogeneity [48], the tumor microenvironment [49], the immune system [50], and metabolic status [51, 52]. Consequently, radiotherapy resistance in cervical cancer is a multifaceted process involving multiple pathways and mechanisms. These mechanisms include enhanced DNA repair, cell cycle arrest, hypoxia responses, increased cell proliferation, inhibition of apoptosis, and autophagy [53].

Ionizing radiation primarily exerts its effects by inducing DNA damage, including double-strand DNA breaks (DSBs), single-strand DNA breaks (SSBs), and DNA crosslinking, with DSBs being the most lethal form of DNA damage [54, 55]. One critical component of the DNA damage response is the phosphorylation of H_2AX, a histone variant, at sites of DSBs, resulting in the formation of γ-H_2AX.

The level of γ-H_2AX is directly proportional to the number of DSBs caused by radiation therapy, making it a widely accepted marker for assessing DSBs [56, 57]. Inadequate DNA repair following radiation-induced damage leads to increased cell death and heightened radiosensitivity.

DNA repair occurs through several mechanisms, including homologous recombination (HR), nucleotide and base excision repair (BER), non-homologous end joining (NHEJ), and telomere metabolism. Among these,

HR and BER are particularly critical for repairing radiation-induced DNA damage. HR is the primary pathway for repairing DSBs, while BER is essential for repairing SSBs [58]. RAD51 plays a central role in HR by mediating the repair of DSBs caused by ionizing radiation and alkylating agents [59].

RAD51 is overexpressed in a range of malignancies, including breast, prostate, bladder, and lung cancers, as well as soft tissue sarcomas [60]. This overexpression enhances HR efficiency, thereby contributing to increased resistance to chemoradiotherapy in tumor cells. Furthermore, elevated RAD51 expression has been identified as an independent predictor of tumor progression and recurrence [61].

In the present study, high expression levels of MICAL2 were observed in irradiation-tolerant cervical cancer cells. Notably, MICAL2 knockdown led to a significant increase in the DNA damage marker γ-H_2AX and a reduction in the DNA repair protein RAD51 following radiotherapy. This heightened level of DNA damage resulted in enhanced radiosensitivity of cervical cancer cells, suggesting that MICAL2 influences the DNA damage response and repair mechanisms critical to tumor resistance to radiotherapy.

There is a growing body of research on gene therapy for tumors; however, the clinical translation of many basic studies remains challenging. Gene therapy technologies for cancer aim to halt tumor growth by introducing transgenes into tumor cells, but significant barriers to clinical application persist.

Small interfering RNAs (siRNAs) have emerged as promising tools in precision medicine for cancer. Unlike traditional small molecule drugs, which are limited to targeting specific protein classes, siRNAs can downregulate the expression of nearly any gene and its corresponding mRNA transcripts, offering broad therapeutic potential [62]. Despite this, unmodified siRNAs face systemic delivery challenges, including poor stability in circulation, suboptimal pharmacokinetics, and limited biodistribution [63].

Viral vectors are commonly used to deliver genes to target cells due to their high transfection efficiency. However, their clinical use is constrained by significant safety risks, such as eliciting strong host immune responses, inflammation, viral reactivation, and even potential disease transmission [64]. To address these limitations, the development of non-viral vectors has gained attention. Non-viral gene delivery methods focus on reducing immune responses and enhancing safety profiles, offering a potentially viable alternative to viral-driven approaches for clinical gene therapy.

Nanotechnology is increasingly recognized as a viable solution to the challenges associated with gene and drug delivery in cancer therapy. By targeting cancer cells with precision, nanotechnology facilitates drug delivery to specific locations, minimizing off-target effects and maximizing therapeutic efficacy [65]. For instance, Jere et al. successfully utilized a biodegradable nanopolymer carrier loaded with AKT1 siRNA, effectively silencing the AKT1 protein, which led to reduced cancer cell survival, proliferation, malignancy, and metastasis [66].

Several nanomedicines have already been approved for anticancer therapy, including Genexol-PM® (a polymeric micellar formulation), Doxil® (liposomal doxorubicin), and Myocet™ (non-pegylated liposomal doxorubicin) [67]. Among the various applications of nanotechnology in medicine, nanoparticles (NPs) play a crucial role in improving drug delivery and enhancing the effectiveness of cancer treatment.

Actively targeted nanoparticles are particularly effective at infiltrating tumors and entering malignant cells [68, 69]. These nanoparticles are often conjugated with molecules targeting tumor-specific surface antigens, such as proteins (e.g., antibodies) [70, 71], aptamers [72], peptides [73], and polysaccharides [74]. Another emerging approach involves the use of external magnetic guidance to direct metal nanoparticles, promoting preferential tumor extravasation [75].

Metal NPs have shown significant promise in enhancing the effectiveness of radiation therapy for cancer treatment. When delivered to tumor sites, NPs improve radiosensitivity by selectively absorbing and scattering high-energy radiation. This enhances radiation therapy uptake efficiency in tumor regions, increases localized damage to tumor cells, and minimizes off-target effects on surrounding healthy tissues [76].

Among metal nanoparticles, silver nanoparticles (Ag-NPs) are particularly notable for their medical applications. Ag-NPs have been demonstrated to induce oxidative stress, DNA damage, apoptotic cell death, and cytokine production [77, 78].

However, conventional methods of synthesizing metal nanoparticles often face significant challenges, including high costs, toxic byproducts, and environmental concerns. To address these issues, green synthesis technologies have emerged as a sustainable alternative. Green synthetic methods use biological sources, such as plant-derived materials, to produce environmentally friendly nanoparticles. For example, pumpkin-derived Ag-NPs offer a promising, natural approach to synthesizing stable and effective metal nanoparticles [76]. The development of green synthetic methods has garnered considerable attention in cancer therapy.

Furthermore, MICAL2 expression levels were found to be inversely correlated with radiotherapy response and positively correlated with the FIGO stage in clinical

patients with cervical cancer. These findings suggest that MICAL2 may serve as a novel target for enhancing radiation sensitivity in cervical carcinoma, although further validation in larger patient cohorts is necessary to establish its clinical relevance.

The implications of this study for biomedical applications are primarily reflected in two key aspects:

Development of MICAL2-targeted strategies: The identification of high MICAL2 expression in cervical cancer and its critical role in tumor progression and radiotherapy resistance provides a robust scientific foundation for developing targeted therapeutic strategies. These strategies could facilitate precision therapy, particularly for patients who exhibit poor responses to conventional radiotherapy.

MICAL2 as a predictive biomarker: The strong association between MICAL2 expression levels and radiotherapy sensitivity highlights its potential as a biomarker for predicting treatment outcomes. By assessing MICAL2 levels, clinicians could tailor treatment plans, improving therapeutic efficacy. Additionally, reducing MICAL2 expression or inhibiting its function may enhance the radiosensitivity of cervical cancer cells, ultimately improving patient outcomes.

Conclusion

This study underscores, for the first time, the pivotal role of MICAL2 in the initiation and progression of cervical cancer, while also elucidating its impact on the radiosensitivity of cervical cancer cells. These findings provide a novel perspective on cervical cancer pathogenesis and therapeutic resistance, offering a theoretical foundation for the development of more effective, targeted treatment strategies.

Abbreviations

MICALs	Molecule interacting with CasL
MICAL2	Molecule interacting with CasL-2
VEGF	Vascular endogenous growth factor
PDGF	Platelet-derived growth factor
EGF	Epidermal growth factor
FGF	Fibroblast growth factor
EMT	Epithelial-mesenchymal transition
EGFR	EGF receptor
ATCC	American Type Culture Collection
FBS	Fetal bovine serum
WB	Western immunoblotting
SDS-PAGE	Sodium dodecyl sulfate–polyacrylamide gel electrophoresis
PVDF	Polyvinylidene fluoride
ERK	Extracellular regulated protein kinases
Bcl-2	B-cell leukemia/lymphoma 2
Bax	BCL2-Associated X Protein
MMP9	Matrix metalloprotein 9
AO/EB	Acridine orange/ethidium bromide
CASP	Comet Assay Software Project
IHC	Immunohistochemical staining
SD	Standard deviation
DEGs	Differential genes
CESC	Cervical squamous cell carcinoma and endocervical adenocarcinoma
CSCs	Cancer stem cells
CR	Complete response
PR	Partial response
SD	Stable disease
PD	Disease progression
FIGO	International Federation of Gynecology and Obstetrics
PFS	Progression-free survival
OS	Overall survival
MO	Monooxygenase
LIM	Lin11, Isl-1, and Mec-3 domains
CH	Calmodulin homologous
CC	C-terminal coil
ROS	Reactive oxygen species
DSBs	Double-stranded DNA breaks
SSBs	Single-stranded DNA breaks
HR	Homologous recombination
BER	Base excision repair

Acknowledgements

We would like to acknowledge the hard and dedicated work of all the staff that implemented the intervention and evaluation components of the study.

Author contributions

Conception and design of the research: Lijuan Zou, Kun Zou. Acquisition of data: Yun Teng, Hongmei Zhao, Yanbin Huang. Analysis and interpretation of the data: Guoqing Xue, Guohui Zhang. Statistical analysis: Hongmei Zhao, Guohui Zhang, Yanbin Huang. Obtaining financing: Yun Teng. Writing of the manuscript: Yun Teng, Guoqing Xue, Wei Guo. Critical revision of the manuscript for intellectual content: Lijuan Zou, Wei Guo, Kun Zou. All authors read and approved the final draft.

Funding

Science and Technology of Liaoning Province (No. 2023-MS-266).

Availability of data and materials

The datasets used and/or analyzed during the current study are available from the corresponding author on reasonable request.

Declarations

Ethics approval and consent to participate

This study was conducted in accordance with the Declaration of Helsinki and received approval from the Ethics Committee of The Second Affiliated Hospital of Dalian Medical University (No 2023067). All animal care and experimental procedures adhered to the National Institutes of Health Guidelines for the Care and Use of Laboratory Animals and were approved by the Animal Care and Ethics Committee of Dalian Medical University (authorization code: 20233228).

Consent for publication

Not applicable.

Competing interests

The author declares that they have no competing interests.

Author details

[1]Department of Radiation Oncology, The Second Affiliated Hospital of Dalian Medical University, No. 467 of Zhongshan Road, Shahekou District, Dalian 116023, China. [2]Department of Radiation Oncology, Shengjing Hospital of China Medical University, Shenyang 110004, China. [3]Department of Immunology, College of Basic Medical Science, Dalian Medical University, Dalian 116044, China. [4]Institute of Cancer Stem Cells, Dalian Medical University, Dalian 116044, China. [5]Department of Radiation Oncology, The First Affiliated Hospital of Dalian Medical University, No. 222 of Zhongshan Road, Xigang District, Dalian 116011, China.

Received: 22 September 2024 Accepted: 30 December 2024
Published online: 11 January 2025

References

1. Ali I, Wani WA, Haque A, Saleem K. Glutamic acid and its derivatives: candidates for rational design of anticancer drugs. Future Med Chem. 2013;5(8):961–78.
2. Bray F, Laversanne M, Sung H, Ferlay J, Siegel RL, Soerjomataram I, et al. Global cancer statistics 2022: GLOBOCAN estimates of incidence and mortality worldwide for 36 cancers in 185 countries. CA Cancer J Clin. 2024; 74(3):229–263.
3. Chen S, Cao Z, Prettner K, Kuhn M, Yang J, Jiao L, et al. Estimates and projections of the global economic cost of 29 cancers in 204 countries and territories from 2020 to 2050. JAMA Oncol. 2023;9(4):465–72.
4. Guida F, Kidman R, Ferlay J, Schüz J, Soerjomataram I, Kithaka B, et al. Global and regional estimates of orphans attributed to maternal cancer mortality in 2020. Nat Med. 2022;28(12):2563–72.
5. Sung H, Ferlay J, Siegel RL, Laversanne M, Soerjomataram I, Jemal A, et al. Global Cancer Statistics 2020: GLOBOCAN estimates of incidence and mortality worldwide for 36 cancers in 185 countries. CA Cancer J Clin. 2021;71:209–49.
6. Arbyn M WE, Bruni L, de Sanjosé S, Saraiya M, Ferlay J, Bray F. Estimates of incidence and mortality of cervical cancer in 2018: a worldwide analysis.
7. Koh W-J, Abu-Rustum NR, Bean S, Bradley K, Campos SM, Cho KR, et al. Cervical cancer, version 3.2019, NCCN clinical practice guidelines in oncology. J Natl Comprehensive Cancer Netw. 2019;17:64–84.
8. Santivasi WL, Xia F. Ionizing radiation-induced DNA damage, response, and repair. Antioxid Redox Signal. 2014;21(2):251–9.
9. Peitzsch C, Tyutyunnykova A, Pantel K, Dubrovska A. Cancer stem cells: the root of tumor recurrence and metastases. Semin Cancer Biol. 2017;44:10–24.
10. Schulz A, Meyer F, Dubrovska A, Borgmann K. Cancer stem cells and radioresistance: DNA repair and beyond. Cancers (Basel). 2019;11(6):862.
11. Moreno-Acosta P, Vallard A, Carrillo S, Gamboa O, Romero-Rojas A, Molano M, et al. Biomarkers of resistance to radiation therapy: a prospective study in cervical carcinoma. Radiat Oncol. 2017. https://doi.org/10.1186/s13014-017-0856-2.
12. Eifel PJ, Winter K, Morris M, Levenback C, Grigsby PW, Cooper J, et al. Pelvic irradiation with concurrent chemotherapy versus pelvic and para-aortic irradiation for high-risk cervical cancer: an update of radiation therapy oncology group trial (RTOG) 90–01. J Clin Oncol. 2004;22(5):872–80.
13. Yadav A, Singh S, Sohi H, Dang S. Advances in delivery of chemotherapeutic agents for cancer treatment. AAPS PharmSciTech. 2021;23(1):25.
14. Karpel HC, Powell SS, Pothuri B. Antibody-drug conjugates in gynecologic cancer. Am Soc Clin Oncol Educ Book. 2023;43: e390772.
15. Beck A, Goetsch L, Dumontet C, Corvaïa N. Strategies and challenges for the next generation of antibody-drug conjugates. Nat Rev Drug Discov. 2017;16(5):315–37.
16. Abdollahpour-Alitappeh M, Lotfinia M, Gharibi T, Mardaneh J, Farhadihosseinabadi B, Larki P, et al. Antibody-drug conjugates (ADCs) for cancer therapy: Strategies, challenges, and successes. J Cell Physiol. 2019;234(5):5628–42.
17. Masters JC, Nickens DJ, Xuan D, Shazer RL, Amantea M. Clinical toxicity of antibody drug conjugates: a meta-analysis of payloads. Invest New Drugs. 2018;36(1):121–35.
18. Zhu Y, Liu K, Wang K, et al. Treatment-related adverse events of antibody–drug conjugates in clinical trials: a systematic review and meta-analysis. Cancer. 2018;129:283–95.
19. Ali I, Alsehli M, Scotti L, Tullius Scotti M, Tsai ST, Yu RS, et al. Progress in polymeric nano-medicines for theranostic cancer treatment. Polymers (Basel). 2020;12(3):598.
20. Lee Byung C, Péterfi Z, Hoffmann FuKun W, Moore Richard E, Kaya A, Avanesov A, et al. MsrB1 and MICALs regulate actin assembly and macrophage function via reversible stereoselective methionine oxidation. Mol Cell. 2013;51:397–404.
21. Cai Y, Lu J, Tang F. Overexpression of MICAL2, a novel tumor-promoting factor, accelerates tumor progression through regulating cell proliferation and EMT. J Cancer. 2018;9:521–7.
22. Barravecchia I, Barresi E, Russo C, Scebba F, De Cesari C, Mignucci V, et al. Enriching the arsenal of pharmacological tools against MICAL2. Molecules. 2021. https://doi.org/10.3390/molecules26247519.
23. Hou ST, Nilchi L, Li X, Gangaraju S, Jiang SX, Aylsworth A, et al. Semaphorin3A elevates vascular permeability and contributes to cerebral ischemia-induced brain damage. Sci Rep. 2015. https://doi.org/10.1038/srep07890.
24. Deng W, Wang Y, Gu L, Duan B, Cui J, Zhang Y, et al. MICAL1 controls cell invasive phenotype via regulating oxidative stress in breast cancer cells. BMC Cancer. 2016. https://doi.org/10.1186/s12885-016-2553-1.
25. Hao J, Shen W, Yu G, Jia H, Li X, Feng Z, et al. Hydroxytyrosol promotes mitochondrial biogenesis and mitochondrial function in 3T3-L1 adipocytes. J Nutr Biochem. 2010;21:634–44.
26. Alto LT, Terman JR. MICALs. Curr Biol. 2018;28:R538–41.
27. Zou X, Feng Z, Li Y, Wang Y, Wertz K, Weber P, et al. Stimulation of GSH synthesis to prevent oxidative stress-induced apoptosis by hydroxytyrosol in human retinal pigment epithelial cells: activation of Nrf2 and JNK-p62/SQSTM1 pathways. J Nutr Biochem. 2012;23:994–1006.
28. Zhou W, Liu Y, Gao Y, Cheng Y, Chang R, Li X, et al. MICAL2 is a novel nucleocytoplasmic shuttling protein promoting cancer invasion and growth of lung adenocarcinoma. Cancer Lett. 2020;483:75–86.
29. Qi C, Min P, Wang Q, Wang Y, Song Y, Zhang Y, et al. MICAL2 contributes to gastric cancer cell proliferation by promoting YAP dephosphorylation and nuclear translocation. Oxid Med Cell Longev. 2021;2021:9955717.
30. Pu B, Zhang X, Yan T, Li Y, Liu B, Jian Z, et al. MICAL2 promotes proliferation and migration of glioblastoma cells through TGF-β/p-Smad2/EMT-like signaling pathway. Front Oncol. 2021;11: 735180.
31. Ashida S, Furihata M, Katagiri T, Tamura K, Anazawa Y, Yoshioka H, et al. Expression of novel molecules, MICAL2-PV (MICAL2 prostate cancer variants), increases with high gleason score and prostate cancer progression. Clin Cancer Res. 2006;12:2767–73.
32. Hong W, Ho JR, Chapeaublanc E, Kirkwood L, Nicolle R, Benhamou S, et al. Deregulation of Rab and Rab effector genes in bladder cancer. PLoS ONE. 2012;7(6): e39469.
33. Wang Y, Deng W, Zhang Y, Sun S, Zhao S, Chen Y, et al. MICAL2 promotes breast cancer cell migration by maintaining epidermal growth factor receptor (EGFR) stability and EGFR/P38 signalling activation. Acta Physiol. 2018;222(2):10.
34. Li Z, Zhang Y, Sui S, Hua Y, Zhao A, Tian X, et al. Targeting HMGB3/hTERT axis for radioresistance in cervical cancer. J Exp Clin Cancer Res. 2020;39(1):243.
35. Valent P, Bonnet D, De Maria R, Lapidot T, Copland M, Melo JV, et al. Cancer stem cell definitions and terminology: the devil is in the details. Nat Rev Cancer. 2012;12:767–75.
36. Abad E, Graifer D, Lyakhovich A. DNA damage response and resistance of cancer stem cells. Cancer Lett. 2020;474:106–17.
37. Li J, Liu H, Li Y, Li J, Shen L, Long W, et al. Comparison of outcomes and side effects for neoadjuvant chemotherapy with weekly cisplatin and paclitaxel followed by chemoradiation vs chemoradiation alone in stage IIB–IVA cervical cancer: study protocol for a randomized controlled trial. Trials. 2022;23(1):29.
38. Giridharan SSP, Rohn JL, Naslavsky N, Caplan S. Differential regulation of actin microfilaments by human MICAL proteins. J Cell Sci. 2012;125:614–24.
39. Frémont S, Romet-Lemonne G, Houdusse A, Echard A. Emerging roles of MICAL family proteins—from actin oxidation to membrane trafficking during cytokinesis. J Cell Sci. 2017;130(9):1509–17.
40. Ortegón Salas C, Schneider K, Lillig CH, Gellert M. Signal-regulated oxidation of proteins via MICAL. Biochem Soc Trans. 2020;48:613–20.
41. Dokmanovic M, Marks PA. Prospects: histone deacetylase inhibitors. J Cell Biochem. 2005;96:293–304.
42. Liu Z, Sun B, Xu A, et al. MICAL2 implies immunosuppressive features and acts as an independent and adverse prognostic biomarker in pancreatic cancer. Sci Rep. 2024;14(1):3177.
43. Barravecchia I, Mariotti S, Pucci A, Scebba F, De Cesari C, Bicciato S, et al. MICAL2 is expressed in cancer associated neo-angiogenic capillary endothelia and it is required for endothelial cell viability, motility and VEGF response. Biochim Biophys Acta BBA Mol Basis Dis. 2019;1865:2111–24.
44. Hellweg R, Mooneyham A, Chang Z, Shetty M, Emmings E, Iizuka Y, et al. RNA sequencing of carboplatin- and paclitaxel-resistant endometrial cancer cells reveals new stratification markers and molecular targets for cancer treatment. Hormones Cancer. 2018;9:326–37.
45. Tao W, Sun W, Zhu H, Zhang J. miR-205-5p suppresses pulmonary vascular smooth muscle cell proliferation by targeting MICAL2-mediated Erk1/2 signaling. Microvasc Res. 2019;124:43–50.

46. Wang Q, Qi C, Min P, Wang Y, Ye F, Xia T, et al. MICAL2 contributes to gastric cancer cell migration via Cdc42-dependent activation of E-cadherin/β-catenin signaling pathway. Cell Commun Signal. 2022;20(1):136.
47. Kageyama S-I, Du J, Kaneko S, Hamamoto R, Yamaguchi S, Yamashita R, et al. Identification of the mutation signature of the cancer genome caused by irradiation. Radiother Oncol. 2021;155:10–6.
48. Marie-Egyptienne DT, Lohse I, Hill RP. Cancer stem cells, the epithelial to mesenchymal transition (EMT) and radioresistance: Potential role of hypoxia. Cancer Lett. 2013;341:63–72.
49. Barker HE, Paget JTE, Khan AA, Harrington KJ. The tumour microenvironment after radiotherapy: mechanisms of resistance and recurrence. Nat Rev Cancer. 2015;15:409–25.
50. Junttila MR, de Sauvage FJ. Influence of tumour micro-environment heterogeneity on therapeutic response. Nature. 2013;501:346–54.
51. Mukha A, Kahya U, Dubrovska A. Targeting glutamine metabolism and autophagy: the combination for prostate cancer radiosensitization. Autophagy. 2021;17:3879–81.
52. Jiang N, Xie B, Xiao W, Fan M, Xu S, Duan Y, et al. Fatty acid oxidation fuels glioblastoma radioresistance with CD47-mediated immune evasion. Nat Commun. 2022;13(1):1511.
53. Porrazzo A, Cassandri M, D'Alessandro A, Morciano P, Rota R, Marampon F, et al. DNA repair in tumor radioresistance: insights from fruit flies genetics. Cell Oncol. 2023. https://doi.org/10.1007/s13402-023-00906-6.
54. Ornish D. Mediterranean diet for primary prevention of cardiovascular disease. N Engl J Med. 2013;369:675–6.
55. Abdel-Fatah T, Sultana R, Abbotts R, Hawkes C, Seedhouse C, Chan S, et al. Clinicopathological and functional significance of XRCC1 expression in ovarian cancer. Int J Cancer. 2012;132:2778–86.
56. Beunza JJ, Toledo E, Hu FB, Bes-Rastrollo M, Serrano-Martinez M, Sanchez-Villegas A, et al. Adherence to the Mediterranean diet, long-term weight change, and incident overweight or obesity: the Seguimiento Universidad de Navarra (SUN) cohort. Am J Clin Nutr. 2010;92:1484–93.
57. De Angelis PM, Schjølberg AR, Hughes JB, Huitfeldt HS, Norheim Andersen S, Østvold AC. Nondysplastic ulcerative colitis has high levels of the homologous recombination repair protein NUCKS1 and low levels of the DNA damage marker gamma-H_2AX. Inflamm Bowel Dis. 2018;24:593–600.
58. Yoo Y, Cho M, Lim J, Lindroth AM, Park YJ. Diet-induced obesity leads to metabolic dysregulation in offspring via endoplasmic reticulum stress in a sex-specific manner. Int J Obes. 2018;42(2):244–51.
59. Gachechiladze M, Škarda J, Soltermann A, Joerger M. RAD51 as a potential surrogate marker for DNA repair capacity in solid malignancies. Int J Cancer. 2017;141:1286–94.
60. Budke B, Lv W, Kozikowski AP, Connell PP. Recent developments using small molecules to target RAD51: how to best modulate RAD51 for anticancer therapy? ChemMedChem. 2016;11(22):2468–73. https://doi.org/10.1002/cmdc.201600426.
61. Nogueira A, Catarino R, Faustino I, Nogueira-Silva C, Figueiredo T, Lombo L, et al. Role of the RAD51 G172T polymorphism in the clinical outcome of cervical cancer patients under concomitant chemoradiotherapy. Gene. 2012;504:279–83.
62. Chen Z, Krishnamachary B, Pachecho-Torres J, Penet MF, Bhujwalla ZM. Theranostic small interfering RNA nanoparticles in cancer precision nanomedicine. Wiley Interdiscip Rev Nanomed Nanobiotechnol. 2020;12(2):e1595.
63. Wang K, Kievit FM, Zhang M. Nanoparticles for cancer gene therapy: recent advances, challenges, and strategies. Pharmacol Res. 2016;114:56–66.
64. Rosic G, Selakovic D, Omarova S. Cancer signaling, cell/gene therapy, diagnosis and role of nanobiomaterials. Adv Biol Earth Sci. 2024;9(Special Issue):11–34.
65. Soni G, Yadav KS. Applications of nanoparticles in treatment and diagnosis of leukemia. Mater Sci Eng C Mater Biol Appl. 2015;47:156–64.
66. Jere D, Arote R, Jiang HL, Kim YK, Cho MH, Cho CS. Bioreducible polymers for efficient gene and siRNA delivery. Biomed Mater. 2009;4(2): 025020.
67. Piktel E, Niemirowicz K, Wątek M, Wollny T, Deptuła P, Bucki R. Recent insights in nanotechnology-based drugs and formulations designed for effective anti-cancer therapy. J Nanobiotechnol. 2016;14:39.
68. Björnmalm M, Thurecht KJ, Michael M, et al. Bridging bio-nano science and cancer nanomedicine. ACS Nano. 2017;11:9594–613.
69. Bahrami B, Hojjat-Farsangi M, Mohammadi H, et al. Nanoparticles and targeted drug delivery in cancer therapy. Immunol Lett. 2017;190:64–83.
70. Hu Y, Liu C, Muyldermans S. Nanobody-based delivery systems for diagnosis and targeted tumor therapy. Front Immunol. 2017;8:1442.
71. Marques AC, Costa PJ, Velho S, et al. Functionalizing nanoparticles with cancer-targeting antibodies: a comparison of strategies. J Controlled Release. 2020;320:180–200.
72. Alshaer W, Hillaireau H, Fattal E. Aptamer-guided nanomedicines for anticancer drug delivery. Adv Drug Deliv Rev. 2018;134:122–37.
73. Zhong Y, Meng F, Deng C, et al. Ligand-directed active tumor-targeting polymeric nanoparticles for cancer chemotherapy. Biomacromol. 2014;15:1955–69.
74. Peng P, Yang K, Tong G, et al. Polysaccharide nanoparticles for targeted cancer therapies. Curr Drug Metab. 2018;19:781–92.
75. Hauser AK, Wydra RJ, Stocke NA, et al. Magnetic nanoparticles andnanocomposites for remote controlled therapies. J Controlled Release. 2015;219:76–94.
76. Montazersaheb S, et al. Green-synthesized silver nanoparticles from peel extract of pumpkin as a potent radiosensitizer against triple-negative breast cancer (TNBC). Cancer Nanotechnol. 2024;15(1):47.
77. Liu Y, Zhang D, Zhang Z, Liang X, Yang X, Ding N, et al. Multifunctional nanoparticles inhibit tumor and tumor-associated macrophages for triple-negative breast cancer therapy. J Colloid Interface Sci. 2024;657:598–610.
78. Montazersaheb S, Farahzadi R, Fathi E, Alizadeh M, Abdolalizadeh Amir S, Khodaei Ardakan A, et al. Investigation the apoptotic effect of silver nanoparticles (Ag-NPs) on MDA-MB 231 breast cancer epithelial cells via signaling pathways. Heliyon. 2024;10(5): e26959.

Publisher's Note

Springer Nature remains neutral with regard to jurisdictional claims in published maps and institutional affiliations.